Materials Advances

ROYAL SOCIETY OF CHEMISTRY

PAPER

View Article Online
View Journal

Cite this: DOI: 10.1039/d5ma01178g

Designing PANI-modified PU films coupled with CNTs for enhanced shape memory properties

Tehmeena Ishaq,[a] Rabia Sattar,*[a] Rabia Naeem,*[b] Mahwish Iqbal[c] and Sana Ullah[d]

Received 12th October 2025,
Accepted 19th May 2026

DOI: 10.1039/d5ma01178g

rsc.li/materials-advances

Polyurethane (PU)-based shape memory polymers are considered a supreme choice for shape recovery applications. However, they face problems with their mechanical and thermal properties, which can lead to significant challenges in their development and practical implications. Herein, an effectual and novel strategy has been adopted to overcome these limitations by incorporating CNTs along with polyaniline into the PU chains to form a ternary PU-based nanocomposite. By introducing these conductive fillers, an exceptional elongation at break (18.35%), a higher thermal stability (up to 342 °C), an optimal Young's modulus (456.49 MPa) and high tensile strength (26.49 MPa) were achieved. However, a higher shape recovery aptitude (97%), higher shape fixity (98%) and an enhanced electrical conductivity of 5.00 × 10^{-2} S cm^{-1} were achieved for the ternary hybrid. Overall, the PANI/f-CNTs@PU nanocomposite designed in the current study depicted ideal shape memory parameters, which can be credited to the combined effect of the CNTs and PANI in the PU matrix. The fabricated nanocomposite PANI/f-CNTs@PU can be further utilized in various memory-based applications of materials in diversified industrial applications, including sensors, self-healing materials, electronics, *etc.*

1 Introduction

The term "smart materials" dates back to the 1980s and became a cornerstone of modern industry owing to their huge variety of applications in the fields of robotics, aerospace, smart manufacturing, biomedicine, artificial intelligence, flexible electronics, *etc.* Smart composite materials are a class of novel materials that provide active responses when subjected to an external stimulus with the functions of self-healing, self-deriving, self-sensing, *etc.*[1] Smart structures and smart materials are machinable structural set-ups which incorporate sensing and control, and actuate various functions. Shape memory polymers (SMPs) are a category of polymeric materials that manifest the unique capability to recover their original dimensions and permanent shape when stimulated by a specific external stimulus, such as magnetism,[2] light,[3] electricity[4] or heat.[5] SMPs can be characterized by their versatile nature with regard to programmable deformation, easy molding, composability and stiffness.[6] SMPs include thermoplastic resins and thermosetting resins such as polycaprolactone, polylactic acid, polystyrene, polyimide, cyanate ester,[7] elium,[8] epoxy resin, and polyurethane.[7]

Among these SMPs, polyurethane (PU) stands out as a promising choice as a shape memory material for different applications due to its structural diversity and tunable nature. PU is well-known for its higher melting point, easy manufacturing and excellent elasticity.[9] Nevertheless, its poor thermal and mechanical properties[10] limit its usage at an industrial scale; however, these properties can be improved by incorporating suitable nanofillers in the polymeric matrix of the PU chains.[11] For instance, Baber *et al.*[12] reported a Bentone/PU clay-based composite and observed a 34% improvement in the glass transition temperature (T_g) with a shift of the degradation temperature to 46 °C compared to pristine PU. Furthermore, the role of carbon nanotubes (CNTs) in enhancing the shape recovery properties of SMPs has been investigated extensively; for example, Gohar *et al.* investigated the tensile strength of MWCNT@PU nanocomposites with 0–1.0 wt% loading of MWCNTs. It was revealed that the elongation at break was improved by 11% while the elastic modulus was increased by 25% and the ultimate tensile strength was increased by about 21% for the 1%MWCNT@PU composite compared to pristine PU.[13] This enhancement in strength and elastic modulus was ascribed to uniform dispersion and interfacial bonding between the PU chains and MWCNTs. In another study, Namathoti *et al.*[14] reported an improvement in the thermal and tensile properties of HNT/MWCNTs@PU. A higher tensile value of 23.5 MPa and a T_g at 69.0 °C were observed for 0.1%

[a] *Department of Chemistry, University of Lahore, Sargodha Campus, Sargodha, 40100, Pakistan. E-mail: ishaqtehmeena@gmail.com, rabiasattar39@yahoo.com*
[b] *Department of Chemistry, Government College University Lahore, Katchery Road, 54000, Pakistan. E-mail: rabianaeem@gcu.edu.pk*
[c] *Department of Chemistry, University of Agriculture, Faisalabad, 38000, Pakistan. E-mail: mahwishiqbal2323@gmail.com*
[d] *Nano Fusion Technology Research Group, Institute for Fiber Engineering (IFES), Interdisciplinary Cluster for Cutting Edge Research (ICCER), Shinshu University, Tokida 3-15-1, Ueda, 386-8567, Nagano, Japan. E-mail: sana_ullah@shinshu-u.ac.jp*

MWCNT loading in the PU matrix. Recently, the interest in PANI-based conducting materials has increased owing to its high environmental stability, effortless synthesis and higher electrical conductivity.[15,16] In addition, there have been reports which manifest that polyaniline mixing with other polymers to form SMP composites results in improvement of the thermal, mechanical and electrical properties. For instance, Wang *et al.* designed a HCNT/PANI/PU-based composite *via* directional freezing and achieved a high degree of shape deformation and shape recovery, which was credited to the hydrogen bonding developed between the PU and PANI network.[17]

Although there have been many reports that reveal the positive impact of CNTs and PANI on the shape recovery properties of PU, there is no reported work on the collective effect of f-CNTs along with PANI on the shape memory properties of the PU matrix to date, to the best of our knowledge. The aim of the current study was to measure the impact of amine functionalized CNTs (f-CNTs) as well as PANI on the electrical, mechanical, thermal and shape recovery properties of the PU matrix by varying the concentration of PANI in the ternary composite material to achieve an optimized SMP that could be employed in the future for diverse shape memory applications with higher electrical conductivity and superior thermal stability at the industrial scale. Hence, our work investigates their combined impact on shape memory, electrical conductivity and mechanical integrity under controlled composition and concentration. Moreover, we demonstrated that low PANI content leads to a non-linear increase in shape memory properties. Additionally, our present work focuses on using a low amount of conductive fillers and non-toxic and cost-effective precursors for SMPs, thereby minimizing the harmful impact on the environment.

2 Materials and methods

2.1 Chemicals used

Polyethylene oxide (PEO, MW = 10^5), poly(propylene glycol)-*block*-poly(ethylene glycol)-*block*-poly(propylene glycol) (PPG-*b*-PEG-*b*-PPG, MW = 2000), 2,4-toluene diisocyanate (TDI, 99%), aniline (99%), multi wall carbon nanotubes (MWCNTs, L = 10–30 μm and D = 10–20 nm), ammonium bicarbonate (NH_4HCO_3), ethanol, potassium dichromate ($K_2Cr_2O_7$), hydrochloric acid (HCl), and tetrahydrofuran (THF, 99.5%) were used. All of these chemicals were purchased from Sigma Aldrich, while THF was acquired from Merck.

2.2 Synthesis of the PU polymer and f-CNTs@PU composite

PU was fabricated *via* an addition polymerization approach as reported by Sattar *et al.*[18] In brief, two polyols (PPG-*b*-PEG-*b*-PPG and PEO) with the ratio of 0.9 : 0.1 were taken in THF solvent (30 mL) and stirred for 1 hour at 40 °C. Afterward, 2,4-TDI (1.5 mL) was poured into the polyols dropwise and the mixture was allowed to stir for 3 hours to obtain the PU solution. The THF solvent was evaporated at ambient temperature to form a PU film (1 ± 0.05 mm thickness).

CNTs were purified and amine functionalized to form f-CNTs according to our previous protocol.[18] For purification, the CNTs were annealed at 400 °C for 0.5 hour in a furnace and then refluxed in aqueous HCl (2% w/v) for 1 hour. Finally, CNTs were filtered and washed with distilled water in order to remove the excess HCl. The filtered CNTs were oven dried at 60 °C for 10 hours and were used for (NH_2) amine functionalization. For this purpose, MWCNTs were mixed with NH_4HCO_3 (in a w/w ratio of 1 : 3) and sonicated in ethanol for 3 hours. The mixture was dried at room temperature with constant stirring. Then the sample was ball-milled at 250 rpm for 4 hours followed by heating at 100 °C for 24 hours to remove the residual gases. The obtained amine modified carbon nanotubes were labeled as f-CNTs and further used in the preparation of f-CNTs@PU and PANI/f-CNTs@PU composites.

For the preparation of the f-CNTs@PU composite, 0.1 g of CNTs was added to THF solvent and sonicated of 1 hour, and labelled as soln-1. Moreover, PU was dispersed in THF and the resulting solution was labeled as soln-2. For composite preparation, 3.0 wt% solution of f-CNTs was poured into the PU solution in THF solvent. Both these solutions were stirred for 12 hours at 40 °C for better dispersion of f-CNTs in the PU matrix. Finally, the product formed was poured into a glass Petri dish and the solvent was evaporated at 30 °C leaving a thin film of f-CNTs@PU composite (thickness of 1 ± 0.05 mm), which was stored for further analysis.

2.3 Synthesis of the PANI/f-CNTs@PU composites

PANI was synthesized *via* single-step oxidative polymerization of aniline by using $K_2Cr_2O_7$ and HCl as an oxidative reagent[18] while the fabrication of the (PANI/f-CNTs@PU) composite was achieved by the combination of both solution blending and chemical *in situ* polymerization methods. For this purpose, 0.1 g of f-CNTs and four weight fractions of PANI (0.1, 0.3, 0.5 and 1%) were dissolved in 20 mL of THF solvent and sonicated for 1 hour at ambient temperature. Then, the PANI/f-CNTs hybrid of each concentration was poured into the PU solution and the reaction mixture was allowed to stir for 12 hours at 40 °C. Finally, the product formed was poured into a Petri dish and solvent dried by evaporation at 25 °C leaving a thin film of PANI/f-CNTs@PU composite (thickness of 1 ± 0.05 mm). The schematic structure of the interaction between PANI, f-CNTs and PU in the ternary composite is shown in Scheme 1, while the synthesis scheme is illustrated in Fig. 1.

2.4 Characterization

For functional group analysis of the PU nanocomposites (PANI/f-CNTs@PU), infrared (IR) spectra were recorded in transmission mode on a Nexus 870 FTIR spectrometer with a scan range of 4000–450 cm^{-1}. Morphological analysis of the fabricated samples was accomplished using a Hitachi S-4800 scanning electron microscope (SEM).

Stress–strain behavior of the fabricated composites was evaluated *via* a universal testing machine (UTM) (Instron 4466) according to the ASTM D638 standard method under a strain rate of 5 mm min^{-1} at 23 °C. To evaluate the thermal stability of

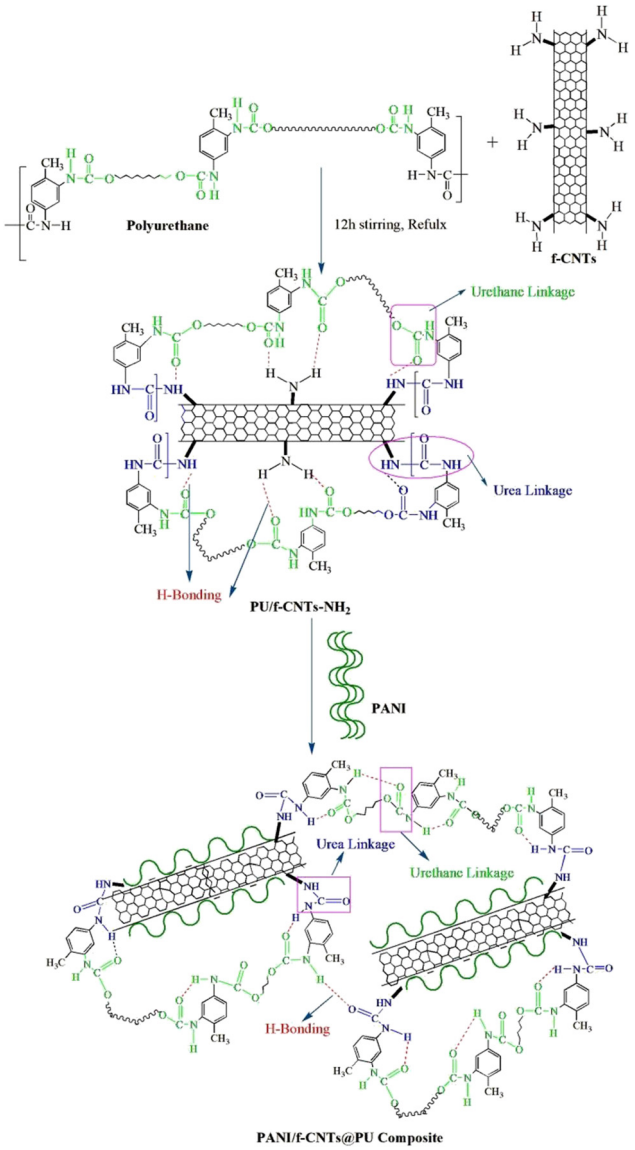

Scheme 1 Probable mechanism of dispersion of PANI and f-CNTs in the PANI/f-CNTs@ PU composite.

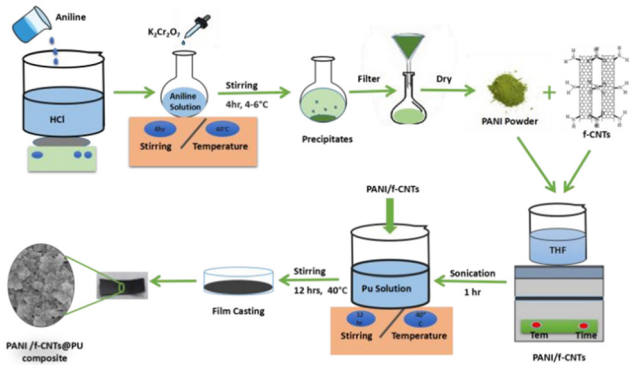

Fig. 1 A schematic presentation of the synthesis protocol followed for the fabrication of the PANI/f-CNTs@PU nanocomposite.

the fabricated materials, thermogravimetric analysis (TGA) was performed on a NETZSCH STA 449 C thermal analyzer. 7–10 mg of the as-synthesized composite was taken in an Al_2O_3 crucible in the temperature range of 25–700 °C with a ramping rate of 20 °C min^{-1} under a nitrogen atmosphere. To investigate the phase transitions of the PU and its PANI-based polymeric films, differential scanning calorimetry (DSC) was performed using a PerkinElmer Pyris 1 DSC (Boston, MA, USA) by taking 5–7 mg of the fabricated samples and using a heating rate of 10 °C min^{-1} in the temperature range of 50–100 °C under an argon atmosphere. To carry out crystallographic analysis, X-ray diffraction (XRD) analysis was performed on a Shimadzu XRD-6000 utilizing crystal monochromatic Cu K_α radiation in the range of $10^\circ < 2\theta < 70^\circ$ at a scan rate of 8° min^{-1}. The electrical conductivity of the composite films was investigated at 25 °C using the four-point technique (Keithley 2400) and rectangular films with dimensions of 35 × 10 × 1 ± 0.05 mm^3 were employed to measure the conductivity according to ASTM D257. By using the V and I readings from the probe, the resistivity of the testing material was calculated as follows:

$$\rho = v/I \times k \quad (1)$$

where k is the geometry-dependent correction factor and is given as:

$$k = A/\ell \quad (2)$$

where ρ shows the resistivity (Ω cm) of the material, w (cm) is the width of the film, ℓ (cm) is the space between the two probes and t (cm) is the film thickness. Knowing the value of resistivity (ρ), the conductivity can be determined as:

$$\sigma = 1/\rho \quad (3)$$

Here, σ represents the electrical conductivity (S cm^{-1}) of the material under the test.

The shape recovery (SR) effect of rectangular films with dimensions of 35 × 10 × 1 ± 0.05 mm^3 was examined by bending the composite films at the transition temperature (T_{trans}), followed by cooling at 20 °C to gain a temporary shape and finally reheating it. The value of T_{trans} for shape memory polyurethane and its ternary nanocomposites was observed at 60 °C, corresponding to T_m obtained from DSC analysis. The shape fixity and recovery were measured from the following eqn (4) and (5).

$$\text{Shape fixation ratio} = (\theta_{fixed}/\theta_{max}) \times 100 \quad (4)$$

$$\text{Shape recovery ratio} = (\theta_{max} - \theta_i/\theta_{max}) \times 100 \quad (5)$$

where θ in degrees demonstrates the angle between a line joining the midpoint and the end of the curved strips and the tangential line at the midpoint of the composite films.

3 Results and discussion

3.1 Fourier transform infrared (FTIR) spectroscopic analysis

The FTIR spectrum of the synthesized PU and its composites is depicted in Fig. 2. The band of medium intensity that appeared

at 3430–3250 cm^{-1} is due to stretching vibrations of N–H groups. Another distinctive intense band of urethane groups appears at 1720 cm^{-1} and corresponds to carbonyl (C═O) stretching. Two peaks at 1539 cm^{-1} and 1022 cm^{-1} are credited to the bending vibration of the N–H group and C–O–C bond. The peak of medium intensity that appeared in the region of 1235 cm^{-1} shows the stretching vibration mode of C–N groups. So, these peaks for C–N, C═O and N–H groups correspond to the presence of urethane units (*i.e.*, –NHCOO) in the synthesized product.[19] Moreover, the presence of the weak isocyanate band at 2353 cm^{-1} indicates the NCO terminated PU chains.[20] The remaining peaks in the spectra are ascribed to the presence of TDI, PPG–PEG–PPG and PEO structures in the backbone of the PU polymer. Details of these peaks are given in Table S1.

The FTIR spectrum (Fig. S1) of the amine functionalized CNTs shows a weak band at 3648–3334 cm^{-1} due to N–H stretching. A broad band at 1237 cm^{-1} indicates C–N stretching of C–NH_2. These results confirm the presence of NH_2 groups on the CNTs' surface. The FTIR spectrum of f-CNT@PU shows that incorporation of amine functionalized CNTs in the PU polymer resulted in the formation of urea linkages in addition to the urethane linkages, which is ascribed to a slight increase in intensity of the bands arising from the stretching vibrations of N–H and C═O groups at 3361 cm^{-1} and 1716 cm^{-1} respectively. This increase in the peak intensities and the appearance of a shoulder peak at lower wavelength indicate the formation of new urea linkages and H–bonded N–H and C═O stretching vibrations. The absence of the NCO band also supports the formation of urea bonds between the NCO groups of PU and NH_2 groups present on the wall of the f-CNTs.[21]

The primary FTIR characteristic bands of the PANI/f-CNTs@PU composite are analogous to the f-CNTs@PU composite spectrum with a small shifting of the characteristic urethane–urea peaks. The N–H and free carbonyl (C═O) stretching vibration appeared at lower frequency values *i.e.*, 3332 cm^{-1} and 1707 cm^{-1}, respectively. This shift in the intensities of the N–H and C═O stretching vibrations suggests that interaction between the PANI and PU chains is suppressed due to the presence of f-CNTs. The hydrogen bonded carbonyl (C═O) stretching vibration peak also shifted towards a lower frequency at 1673 cm^{-1}, which may indicate the presence of a H-bonded urethane–carbonyl vibration and is responsible for the effective interaction among all three moieties.[22] Predominantly, all other characteristic bands of the pure PU, f-CNT@PU and PANI/f-CNT@PU with their characteristic frequencies are summarized in Table S1. The presence of these bands at various specified intensity values is in good agreement with the FTIR results of PU, f-CNTs and PANI, which reveals successful formation of the PANI/f-CNT@PU ternary composite.

3.2 Morphological investigation

Fig. 3 and Fig. S2 show the SEM microphotographs of pristine PU, f-CNTs@PU, the 0.1%PANI/f-CNTs@PU composite and the 1.0%PANI/f-CNTs@PU composite(s). Fig. 3(a) reveals the homogeneous surface of pristine PU and is defined as a smooth fracture[23] while Fig. 3(b) clearly shows that f-CNTs are uniformly distributed in the polymeric matrix. The polymer-integrated CNTs are shown as bright dots in the micrographs. Furthermore, it is noteworthy here that there was no aggregation in the composite, which is an outcome of amine crafting on the CNTs that offers stronger interaction between the nanotubes and matrix.[24] The amine groups seemed to stabilize the nanotube dispersion by developing urea linkages with the –NCO groups present in the PU matrix. Elemental analysis (Fig. S3) also confirms the presence of C, N, and O with a weight ratio of 67.27, 18.21 and 14.53, respectively, further strengthening the evidence for the presence of the NCO group. This quite fine distribution of the f-CNTs is credited to the chemical (urea linkages) and physical (hydrogen bonding) interactions between the modified nanotubes and the polymer matrix, as depicted in the proposed reaction mechanism (Scheme 1).

It is a known fact that the presence of an agglomeration of the nanofiller in the matrix depreciates the thermal and mechanical properties of the nano-composites. Here, the quite

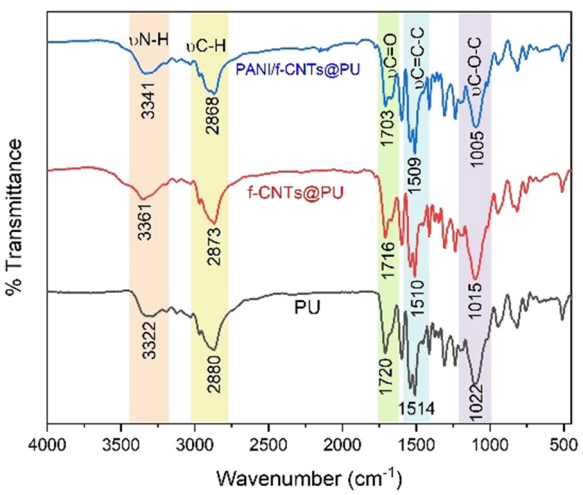

Fig. 2 FTIR spectrum of the PANI/f-CNTs@PU composite.

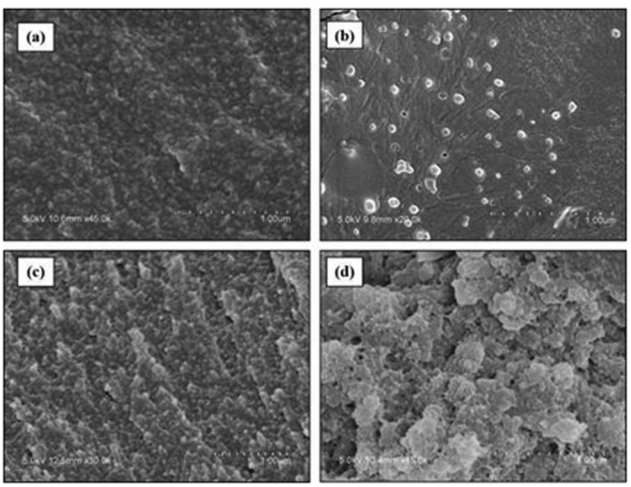

Fig. 3 SEM images of: (a) PU; (b) f-CNT@PU; (c) 0.1%PANI/f-CNTs@PU; (d) 1.0%PANI/f-CNTs@PU at 1 μm.

good dispersion of f-CNTs in the PU matrix can offer improved mechanical, thermal and shape memory properties to the PU matrix.

The SEM micrograph of the PANI/f-CNTs@PU composite with 0.1 and 1.0 wt% of PANI is shown in Fig. 3(c and d). It was revealed that the insertion of PANI created a short tubule-like structure with a flaky appearance, which could be uniformly dispersed in the PU polymeric matrix. Moreover, the fracture surface of the polymeric matrix was found to be more rough, entangled and more flaky with an increase in concentration of PANI from 0.1% to 1.0% in the PANI/f-CNTs@PU composite.[23] This fractured surface is accountable for the mechanical strength of the fabricated nanocomposite[25] and validates the results of mechanical strength as shown in Fig. 4 (mechanical strength).

3.3 Stress–strain analysis

The impact of PANI concentration on the ultimate tensile strength and Young's modulus of the f-CNTs@PU based ternary composites is depicted in Fig. 4. The mechanical properties for the pristine PU strips were poor owing to the presence of entangled polyol soft segments.[26] However, the addition of f-CNTs into the PU matrix enhanced the Young's modulus and tensile strength of the PU matrix.[27] On the addition of 3 wt% of f-CNTs in the PU matrix, the tensile strength and Young's modulus of the composite increased from 16.36 ± 0.49 MPa in pure PU to 21.16 ± 0.63 MPa (an increase of 29%) and 299.29 ± 8.98 to 423.79 ± 12.71 MPa (an increase of 42%), respectively. The improved mechanical properties of this binary composite can be credited to the strong interfacial interaction of f-CNTs with the PU chains.[28] Additionally, the amine functional groups on the CNTs are also helpful in the formation of urea linkages.[29] Therefore, these interactions between the f-CNTs and the PU matrix significantly improved the dispersion as well as the interfacial adhesion, resulting in strengthening of the overall mechanical performance of the nanocomposite.[28]

In the case of the PANI/f-CNTs@PU composites, the incorporation of 0.1 wt% PANI content to the f-CNT@PU resulted in an increase of about 53% in Young's modulus and 50% in tensile strength values compared to the neat one. The improved mechanical strength of the nanocomposite can be ascribed to the good dispersal of PANI content in the f-CNT@PU matrix as well as strong interfacial interaction between PANI and the f-CNT@PU polymer matrix. However, for the sample with higher content of PANI (1.0%PANI/f-CNTs@PU), lower values for tensile strength (13.65 ± 0.41 MPa) and Young's modulus (324.44 ± 9.73 MPa) were determined. The observed decrease in the material' strength is due to the presence of agglomerates in these composites, resulting from the layered adsorption of PANI chains on the nanotube wall and less interaction of f-CNTs with the PU matrix.[20] The stress–strain properties of the PU polymer, f-CNTs@PU and PANI/f-CNTs@PU nanocomposite(s) calculated from stress–strain values are summarized in Table S2.

3.4 Thermogravimetric analysis

The effect of f-CNTs and PANI filler on the thermal stability of the PU matrix was examined *via* TGA as shown in Fig. 5. The energy of covalent bonds that constitute the polymeric network in a polymer matrix as well as chemical/physical interaction among the filler and polymeric matrix are the fundamental factors that influence the thermal stability of the nanocomposite.[30] All TGA curves comprising neat PU and its nanocomposite(s) showed a two-stage degradation due to the soft and hard segments in PU. The maximum degradation temperature for the first and second stage of pristine PU were around 410 and 482 °C, while those of the f-CNTs@PU nanocomposite were at 413 and 486 °C, respectively (Table S3). This increase in degradation temperature for the nanocomposite can be ascribed to f-CNT interaction with PU and decreased PU chain thermal motion.[27]

Furthermore, it was revealed that PANI insertion to f-CNT@PU also enhanced the degradation temperature of the polymeric matrix in PANI/f-CNTs@PU. Similarly, an increase in onset temperature up to 342 °C was observed with the increase of the PANI concentration from 0.1 to 1.0 wt%, which can be ascribed to the combined effect of f-CNTs and PANI capitalizing on the presence of interfacial and H-bonding in the PU-based ternary polymeric material.[31] Additionally, higher char residue was also found for the nanocomposite, which may offer higher thermal stability as revealed by many studies in the literature.[32,33]

3.5 Differential scanning calorimetry

The DSC heating and cooling traces of PU and its nanocomposite are displayed in Fig. 6(a & b), respectively. The melting

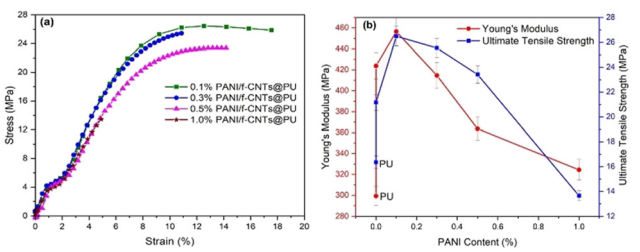

Fig. 4 Impact of PANI concentration on: (a) ultimate tensile strength and (b) Young's modulus of the f-CNTs@PU based ternary composites.

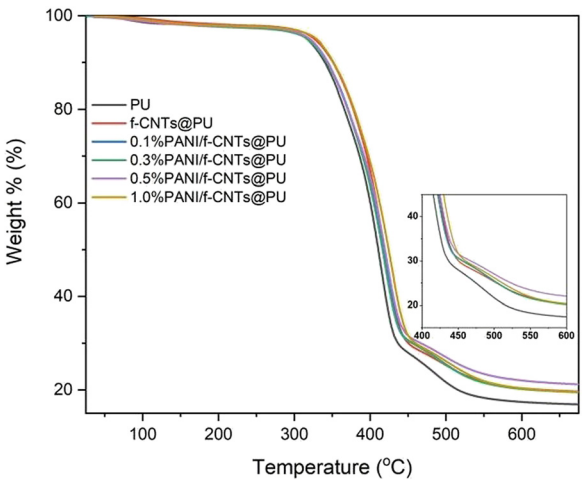

Fig. 5 TGA curves for the PU, f-CNTs@PU and PANI/f-CNTs@PU composite films.

temperature (T_m), glass transition temperature (T_g), crystallization temperature (T_c), heat of crystallization (ΔH_c) and heat of melting (ΔH_m) obtained from DSC analysis are summarized in Table S4.

It was observed that the melting and crystallization temperatures increased with the addition of f-CNTs into the PU matrix. The melting temperature for the neat PU appeared at around 57 °C and only 2 °C rises in T_m were determined for the f-CNTs@PU nanocomposite. Yet, a considerable shift was ascertained in the crystallization behavior. The incorporation of f-CNTs in the PU matrix results in a rise of about 18 °C in crystallization temperature in comparison to neat PU. This was ascribed to H-bonding (–NH groups from the urethane linkages with the >C═O group of the hard segments or with the –O– of the soft segments) and urea linkages (between $–NH_2$ from f-CNTs and –NCO of PU). Besides this nucleating outcome of f-CNTs in the composite is also evident from the rise in T_c and T_m (Fig. 6a). Furthermore, the melt as well as crystallization enthalpies for the nanocomposite were also enhanced compared to pure PU. These findings indicated that the cross-linking was also responsible for an increase in T_g of f-CNTs@PU as displayed in Fig. 6. Good dispersion of f-CNTs in the PU matrix may hinder the molecular motion of the polymeric chains, which could be responsible for an increased T_g of the nanocomposite.[19]

In the case of the PANI/f-CNTs@PU composites, the incorporation of PANI increased the melting and crystallization temperatures in the composites at a lower loading. The effect was more significant in the composite having 0.1% PANI (0.1%PANI/f-CNTs@PU). The highest value of T_g was also obtained for the nanocomposite with 0.1% PANI as shown in Fig. 6. Further increase in the polyaniline content up to 1.0 wt% resulted in a decrease in T_m, T_c and T_g, and a lower heat of melting as well as crystallization. This may be ascribed to the surface overlapping of PANI chains on the walls of the f-CNTs and less interaction of PANI with the PU matrix. This could increase the PU chains' flexibility and phase incompatibility, which in turn are responsible for the decreased DSC parameters with higher loading of PANI in the nanocomposites.

3.6 X-ray diffraction

Fig. 7 depicts the XRD patterns of the PU, f-CNTs@PU and PANI/f-CNTs@PU nanocomposites. PU has a broad but a low intensity peak in the form of a hump with a maximum at 21° (2θ) corresponding to (110) indices, which reveals its slight amorphous nature. This amorphous nature is a result of the randomized orientation of methyl groups connected to PU linkages in the pristine PU.[34,35] It is clear from Fig. 7(b) that the incorporation of f-CNTs improved the crystallinity of the PU. Though the position of the PU peak remained unchanged, the intensity of the hump is slightly increased, which can be credited to the nucleation effect of f-CNTs.[34]

All four concentrations of the PANI/f-CNTs@PU composite (0.1, 0.3, 0.5 and 1.0%) also showed a broader and weaker peak (21°) at a similar position as observed in the pristine PU and f-CNTs@PU which reveals that insertion of PANI did not affect the position of the crystallographic plane (110) of the PU. However, a slight increase in peak intensity was observed with an increase in concentration of PANI, which is due to the semi-crystalline nature of PANI.[36] Hence, this semi-crystalline nature of PANI showed a slight improvement in the structure of f-CNTs@PU, which can offer improved electrical and thermal properties.[31,37]

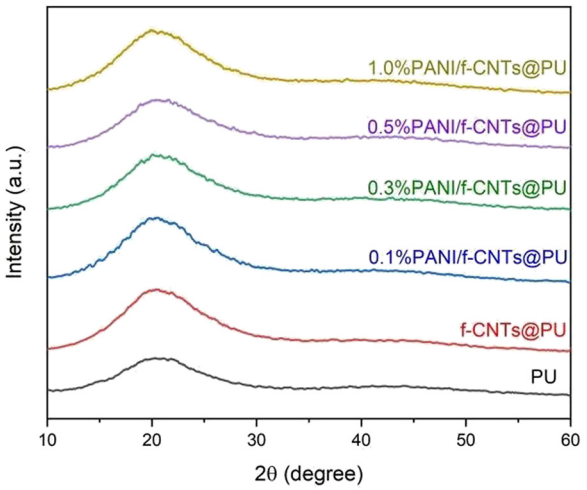

Fig. 7 XRD patterns for the PU, f-CNT@PU, and PANI/f-CNTs@PU composite (0.1, 0.3, 0.5 and 1.0% loading of PANI).

3.7 Electrical conductivity measurement

The influence of f-CNTs and PANI on the electrical conductivity of the fabricated PU films was examined and the results are demonstrated in Table S5. For the PU matrix alone, the electrical conductivity was 4.06×10^{-7} S cm^{-1}, and it raised to 5.30×10^{-6} S cm^{-1} by the insertion of f-CNTs. This value is in the range of 10^{-6} S cm^{-1}, which is a prerequisite for the antistatic properties of the materials for various applications.[38] This improvement in the electrical conductivity of the nanocomposite on loading f-CNTs is ascribed to the good dispersion of nanotubes that resulted in conductive network formation in the PU matrix.

For PANI/f-CNTs@PU composites, the electrical conductivity values were found in the range between 1.68×10^{-4} and 5.00×10^{-2} S cm^{-1} on addition of 0.1–1.0 wt% of PANI. The impact of PANI content on the PANI/f-CNTs@PU nanocomposites is displayed in Fig. 8(b). These values are in the range of 10^{-4}–10^{-2} S cm^{-1} suggesting the formation of conductive networks that are

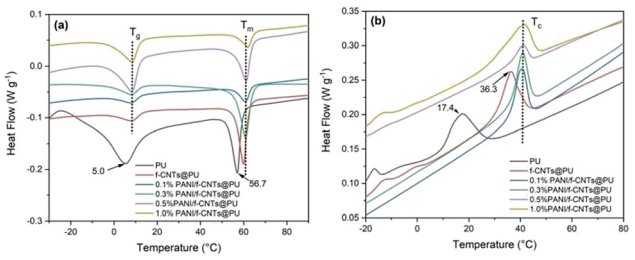

Fig. 6 DSC thermograms showing: (a) melting temperature (T_m) and glass transition temperature (T_g) and (b) crystallization temperature (T_c) for PU, f-CNTs@PU and PANI/f-CNTs@PU composite films.

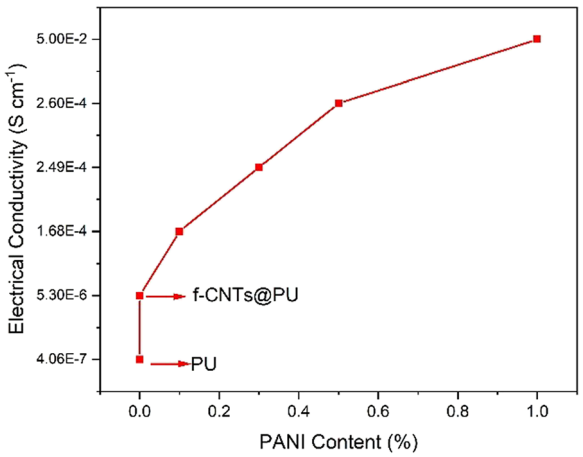

Fig. 8 The impact of PANI concentration on the electrical conductivity of pristine PU in the PANI/f-CNTs@PU composite films.

a prerequisite for electromagnetic shielding (EMI)-based applications as reported in the literature.[39,40] The improved conductivity of the nanocomposite films is credited to the formation of conductive PANI chains over the nanotube interconnected phase in the insulating PU matrix and it is in good agreement with the morphological structure as depicted in the SEM micrograph of Fig. 4(d). The 1.0% PANI/f-CNTs@PU composite revealed a higher value of conductivity (5.00×10^{-2} S cm^{-1}) compared to other nanocomposite films, which indicates a 100-fold increase. Hence, it was found that increased content of PANI in the PU matrix reinforced the conducting bridges in the f-CNT@PU hybrid, which leads to improved electrical conductivity.

3.8 Shape memory study

To evaluate the shape memory properties (*i.e.*, shape recovery and shape fixity), PU-based films were bent at the transition temperature (T_{trans}) and then cooled at ambient temperature (20 °C) to gain temporary shape and lastly heated again. The value of T_{trans} for pure PU and its nanocomposite was around 60 °C, revealing the T_m values shown from DSC analysis. Since the glass transition temperature is low and difficult to control at T_g, this shape memory belongs to T_m-type.[18] The PU and f-CNTs@PU nanocomposite showed a prompt response to recover its original shape within 60 sec as listed in Table S5.

For pure PU, 87% shape fixity was determined during the first cycle while shape memory fixity of 88% appeared for the f-CNTs@PU nanocomposite as depicted in Fig. 9(a). The nanocomposites of PANI/f-CNT@PU showed higher shape fixity as compared to pure PU and f-CNT@PU. For 0.1%PANI/f-CNT@PU, 91% shape fixity was determined while maximum shape fixity (98%) was achieved for 1.0%PANI/f-CNT@PU (1.0 wt% PANI). During the second cycle, the shape fixity values were reduced to 85, 86, 89, 91, 93, and 97 while for the third heating cycle, a further decrease in shape fixity was found in the order of 82, 85, 87, 89, 90, and 95 for pure PU, f-CNT@PU, 0.1%PANI/f-CNT@PU, 0.3%PANI/f-CNT@PU, 0.5%PANI/f-CNT@PU, and 1.0%PANI/f-CNT@PU, respectively. The results of the shape fixity values

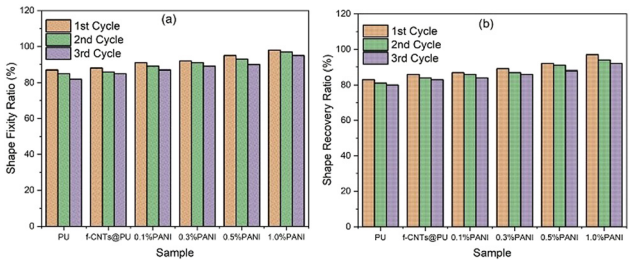

Fig. 9 The impact of PANI concentration on: (a) shape fixity and (b) shape recovery of pristine PU in PANI/f-CNTs@PU composite films over three cycles.

of all PU-based films over three heating cycles are shown in Fig. 9(b).

Additionally, similar increasing shape recovery results were achieved with the addition of PANI to the PU matrix. Fig. 9(b) shows the shape recovery properties of all the fabricated films over three heating cycles. For pristine PU, 83.0% shape recovery was determined while shape memory recovery of 86% appeared for the f-CNTs@PU nanocomposite during the first heating cycle as depicted in Fig. 9(b). It is clear that CNT incorporation enhanced the shape recovery of the PU chains by developing urea linkages and H-bonding.[41]

The nanocomposites of PANI/f-CNT@PU showed higher shape recovery values as compared to pristine PU and f-CNT@PU. For 0.1%PANI/f-CNT@PU, 87% shape recovery was determined while maximum shape recovery (97%) appeared for 1.0%PANI/f-CNT@PU (1.0 wt% PANI) as shown in Fig. 9(B) and 10(C & D). It is obvious that the integration of PANI along with f-CNTs led to a considerable improvement in shape memory due to layered adsorption of PANI chains on the surface of f-CNT@PU and strengthened the polymer networks *via* chemical and physical interactions. Accordingly, a high degree of soft segment crystallinity contributes to higher electrical conductivity, which in turn offers a high shape recovery performance of the composites. Furthermore, during the second cycle, shape recovery values were found to be 81, 84, 86, 87, 91, and 94%, while for the third heating cycle, the shape memory percentage was found to be 80, 83, 84, 86, 88, and 92% for pure PU, f-CNT@PU, 0.1%PANI/f-CNT@PU, 0.3%PANI/f-CNT@PU, 0.5%PANI/f-CNT@PU, and 1.0%PANI/f-CNT@PU, respectively.

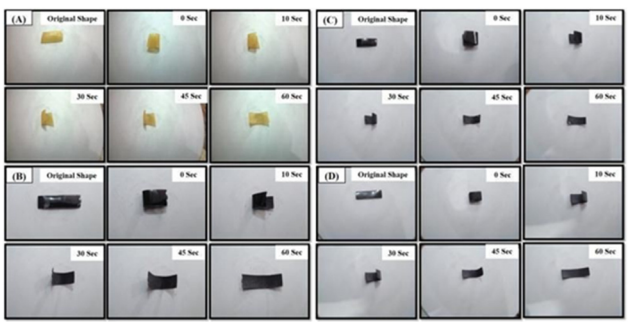

Fig. 10 Shape memory recovery of: (A) PU; (B) f-CNT@PU; (C) 0.1%PANI/f-CNT@PU; (D) 1.0%PANI/f-CNT@PU.

These three cycle shape fixity and shape recovery results indicate that PANI/f-CNT@PU films retain a higher shape memory performance with only a 3% reduction in shape fixity and 5% reduction in shape recovery, showing excellent cycle to cycle stability. This minor reduction can be indicative of polymeric chain rearrangements and stress relaxation during repeated heating cycles.

4 Conclusions

In the current work, we designed a PU-based ternary composite *via* a facile solution blending approach that has homogeneous morphology due to the fine dispersion of modified nanotubes attributed to the formation of urea linkages (reaction N–H of PANI and –NCO of PU), which accounts for the improved mechanical properties and degradation temperature. The fabricated composite film fruitfully attained the coexistence of desirable electrical performance, shape recovery and shape fixity for its practical utility. The DSC studies revealed that the addition of PANI up to 1.0 wt% increased the T_g, T_m and T_c owing to cross-linking along with chain rigidity. An excellent shape recovery effect of about 97% was determined in the composite (1.0%PANI/f-CNTs@PU), which demonstrated that higher PANI content improved the shape memory capability of the PU matrix. The prepared nanocomposites with significant shape recoverability and electrical conductivity values in the range of 10^{-6}–10^{-2} S cm^{-1} could lead to an excellent performance at an industrial scale for a variety of applications, including sensors, self-healing materials, electronics, *etc.*

Author contributions

T. I. and R. S. conceptualization, methodology, original draft writing and writing—review and editing. R. N. and S. U.: conceptualization, methodology, review and editing. R. S.: Investigation, formal analysis. T. I.: investigation, supervision and supporting work. M. I.: writing, visualization and software. T. I.: visualization and software. R. S. and R. N.: conceptualization, supervision, review and editing.

Conflicts of interest

There are no conflicts to declare.

Data availability

The data supporting this article have been included as part of the supplementary information (SI). Supplementary information is available. See DOI: https://doi.org/10.1039/d5ma01178g.

References

1 L. Luo, F. Zhang, L. Wang, Y. Liu and J. Leng, *Adv. Funct. Mater.*, 2024, **34**, 2312036.
2 L. Luo, F. Zhang and J. Leng, *Compos. Sci. Technol.*, 2021, **213**, 108899.
3 H.-X. Wang, X.-Y. Zhao, J.-Q. Jiang, Z.-T. Liu, Z.-W. Liu and G. Li, *ACS Appl. Mater. Interfaces*, 2022, **14**, 51244–51252.
4 S. Zhao, Y. Fan, R. Yang, Z. Ye, F. Zhang, C. Wang, W. Luo, Y. Wen and J. Zhou, *Opto-Electron. Adv.*, 2025, **8**, 240109–240101–240109–240109.
5 X. Xiao, D. Kong, X. Qiu, W. Zhang, F. Zhang, L. Liu, Y. Liu, S. Zhang, Y. Hu and J. Leng, *Macromolecules*, 2015, **48**, 3582–3589.
6 X. Du, F. Zhang, L. Hu, L. Luo, Z. Liu, Y. Liu and J. Leng, *Composites, Part A*, 2025, **190**, 108595.
7 V. Aswany, R. Parvathy, D. Mottammal, S. A. Thomas, J. Cherusseri, D. Kumar, A. Kumar and D. N. Rajendran, in *Polymer Nanocomposites for 3D, 4D and 5D Printing: Fundamental to Applications*, Springer, 2025, pp. 213–240.
8 M. A. Senyurt, M. M. Kurdis, H. Ulus and A. Avcı, *Fibers Polym.*, 2025, **26**, 2097–2116.
9 L. Chen, Z. Xu, M. Gong, L. Zhang, D. Wang, H. Zhou and X. Lin, *Chem. Eng. J.*, 2025, **510**, 161504.
10 S. Gopinath, N. N. Adarsh, P. Radhakrishnan Nair and S. Mathew, *Polym. Compos.*, 2023, **44**, 4433–4458.
11 R. Sanaka and S. K. Sahu, *Heliyon*, 2024, **10**, e24014.
12 M. Babar, A. Sharma, P. Kakkar, A. Arora, T. Arora and G. Verma, *Prog. Org. Coat.*, 2022, **165**, 106743.
13 G. A. Gohar, A. Akhtar, H. Raza, G. Mustafa, M. Fatima, H. U. Rehman, M. W. Aslam, A. ul Haq and W. Manzoor, *Nano Express*, 2023, **4**, 045013.
14 S. Namathoti and M. R. K. Vakkalagadda, *Polymers*, 2023, **15**, 710.
15 H. Du, S. Liu, F. You, J. Wang, Z. Ren and Z. Wu, *Prog. Nat. Sci.: Mater. Int.*, 2021, **31**, 557–566.
16 A. Zotti, S. Aprano, A. Rafiq, S. Zuppolini, M. Zarrelli, M. G. Maglione, P. Tassini, A. Cassinese and A. Borriello, *Mater. Adv.*, 2025, **6**, 1788–1793.
17 H.-Y. Wang, D. Liu, K. Zhang, C. Qian, Y. Dong, N. Jamaluddin, J. Matmin and Y. Zhu, *J. Alloys Compd.*, 2025, 181930.
18 R. Sattar, A. Kausar and M. Siddiq, *Chin. J. Polym. Sci.*, 2015, **33**, 1313–1324.
19 Y. Yin, C. Guo, W. Li, H. Liu and Q. Mu, *Compos. Commun.*, 2024, **50**, 102017.
20 Z. Yan, Y. Liu, Y. Cao, G. Quan, W. Li, D. Li, Y. Wu, L. Xiao and F. Yu, *J. Appl. Polym. Sci.*, 2024, **141**, e55653.
21 R. Wang, H. Wu, R. Chen and Y. Chi, *Small*, 2019, **15**, 1901550.
22 K. Baidya, A. Roy and K. Das, *Mater. Today Commun.*, 2025, **47**, 112979.
23 X.-Z. Tian, R. Yang, J.-J. Ma, Y.-H. Ni, H.-B. Deng, L. Dai, J.-J. Tan, M.-Y. Zhang and X. Jiang, *Chin. J. Polym. Sci.*, 2022, **40**, 789–798.
24 M. Sabet, *Polym.-Plast. Technol. Mater.*, 2025, **64**, 465–494.
25 Y. H. Jo, H. Jung, S. Jeon, H. Choi, H.-W. Kim and H. Sung, *J. Mater. Res. Technol.*, 2025, **36**, 5696–5706.
26 Y. Liu, J. Li, L. Jia, M. Li, Y. Diao, Z. Han, C. Yu and T. Liu, *Mater. Des.*, 2025, **250**, 113611.
27 M. Bidshahri, A. Ameri, M. Sharif and A. Ranjbar, *Int. J. Polym. Sci.*, 2025, **2025**, 4505715.
28 G. Neeraja Rani, R. Panthagani and M. Kanaka Durga, *Mater. Res. Innovations*, 2025, **29**, 129–134.
29 S. Zhang, Y. Xiong, Y. Wang, Y. Ma, J. Li, C. Jiang, C. Wang, Y. Zhu, Y. Zhao and G. Zhang, *Polym. Int.*, 2024, **73**, 874–882.

30 Y. Yao, S. Jin, X. Ma, R. Yu, H. Zou, H. Wang, X. Lv and Q. Shu, *Compos. Sci. Technol.*, 2020, **200**, 108457.
31 B. Gai, S. Li, J. Zhang, Z. Jiang, G. Xie, J. Zhang, S. Xing and M. Yao, *J. Appl. Polym. Sci.*, 2024, **141**, e55761.
32 M. Yang, T. Wang, Y. Tian, H. Zhang, J. Zhang and J. Cheng, *Green Chem.*, 2024, **26**, 4771–4784.
33 H. Chen, G. Ji, F. Lan, Z. Wang, C. Chen, J. Luan, C. Dong and Z. Lu, *Int. J. Biol. Macromol.*, 2024, **270**, 132330.
34 T. C. Codau and E. Codau, *Mater. Today Sustainability*, 2024, **27**, 100831.
35 A. Shahzaib, S. A. Hamdani, R. Mehndi, S. Anjum, S. M. Alshehri, T. Ahamad and N. Nishat, *Inorg. Chem. Commun.*, 2025, 114644.
36 S. V. Ebadi, M. Asadolahi and S. J. Mousavifard, *Microchem. J.*, 2025, 114173.
37 N. Bora, D. P. Joshi and J. S. Aulakh, *Polym. Bull.*, 2024, **81**, 1597–1621.
38 Y. Yang, L. Zhang, S. Ge, H. Huo, K. Huang, M. Rezakazemi and Z. Zhang, *J. Mater. Chem. A*, 2025, **13**, 15075–15087.
39 M. Siri, M. Chandrashekara, B. Hareesh and K. Nandan, *Synth. Met.*, 2025, 117937.
40 M. D. Ali, A. Aslam, M. A. Haider, U. Fakhar, S. Ezzine and H. Somaily, *Inorg. Chem. Commun.*, 2022, **146**, 110039.
41 W. Liu, S. Yang, L. Huang, J. Xu and N. Zhao, *Chem. Commun.*, 2022, **58**, 12399–12417.